Studies of supersonic mixing

By N. T. Clemens AND M. G. Mungal

This report describes studies of supersonic mixing which have been accomplished over the last year with CTR support. During this period, a Nd:Yag laser, optical components, and data acquisition computer were obtained. This allowed detailed visualizations of the flow structure to be performed at a rapid rate, representing a significant improvement over our previous attempts. Aspects of the flow structure are described below. In addition, preliminary findings on a possible mixing enhancement strategy are also shown using the flow visualization technique.

1. The visualization technique

The technique developed in this work uses planar laser Mie scattering from fine alcohol droplets seeded into the flow. Figure 1 shows a schematic of the supersonic wind tunnel. The high-speed side (side 1) is capable of a maximum Mach number of 2.5, while the low-speed side (side 2) is capable of a maximum Mach number of 1.0. Optical access is provided from all sides. The test section pressure is about 10-12 psia, with both stagnation temperatures about 300K.

Two visualization approaches were developed. In the first, alcohol (ethanol) is injected far upstream into side 2. The alcohol vaporizes and uniformly mixes with the low-speed fluid. Upon mixing with the cold high-speed fluid in the mixing layer, condensation of fine alcohol droplets occur and mark the mixing region. This technique is called the "product formation" technique in analogy to chemically reacting systems.

An alternate technique is to seed the alcohol far upstream into side 1. Here, droplets are formed in the supersonic nozzle and uniformly mark the high-speed fluid. The concentration of droplets owing to dilution with the low-speed fluid then decreases across the mixing layer region. This technique is called the "passive scalar" technique in analogy to mixing studies using passive scalars.

Several studies were made to determine the droplet diameters and number densities of the alcohol "fog". Clemens & Mungal (1991a) describe these measurements in some detail and conclude that the diameters were less than 0.2 micron, but are more likely closer to 0.05 micron. Number densities were about $10^{12}/\mathrm{cm}^3$. Using the conservative estimate of diameter, we are able to easily meet the criterion of Samimy & Lele (1990) for proper flow visualizations, in the sense that the particles accurately track the flow. Three additional issues related to visualizations concern: (1) droplet evaporation in the passive scalar case, (2) finite rate formation effects in the product formation case, and (3) droplet coagulation in both cases. It is concluded in Clemens and Mungal (1991a) that while these effects are at play, they are relatively small and do not significantly bias the visualizations to be presented next. Using the current laser and digital camera approach, Fig. 2, we are able to acquire

images to video at about 10 Hz and to computer memory at 3 Hz. Computer storage eliminates film processing which greatly shortens processing time, while digital data allows ease of image processing.

2. Results

Figures 3-6 show visualizations of a low compressibility case using both techniques. Figure 3 shows a schlieren image extending from the splitter tip to 45 cm downstream (0 to 3000 initial momentum thicknesses downstream). Observe that the Brown-Roshko rollers appear past the $x = 15$ cm station. The flow conditions are: $M1 = 1.6$, $M2 = 0.9$, $U1 = 430$ m/s, $U2 = 275$ m/s resulting in a convective Mach number of $Mc = 0.28$ (Papamoschou & Roshko, 1988). To remove the spatial integration of the schlieren, Fig. 4 shows a portion of the flow extending from 15 to 28 cm downstream. Both techniques clearly reveal the Brown-Roshko structure. Plan views of the central 5 cm of the test section are shown in Fig. 5. (The full span of the test section is 10 cm). The product formation technique reveals the two-dimensionality of the Brown-Roshko rollers. The passive scalar approach is best at revealing regions where high-speed fluid is in close proximity to low-speed fluid, namely the braid regions. Careful examination reveals the instantaneous streamwise structure seen in incompressible flows. Finally, Fig. 6 shows end views of the flow in which the core and the braid are captured. The images are consistent with the side and plan views.

Figures 7-10 show analogous photos for a compressible case, $Mc = 0.62$. The flow conditions are: $M1 = 2.0$, $M2 = 0.4$, $U1 = 480$ m/s, and $U2 = 130$ m/s. The most obvious difference is the lack of two-dimensional organization as compressibility increases, and an apparent increase in three-dimensionality. Figure 10 shows that for the compressible case the layer generally appears to be of similar thickness as opposed to the thick core and thin braid seen earlier. The changes to structure are also not a Reynolds number effect as we are able to match Reynolds numbers at different convective Mach numbers and still demonstrate the changes seen here. These results are also generally consistent with the work of Sandham & Reynolds (1989) who predict an increase in three dimensionality with increasing compressibility. Additional photos at $Mc = 0.79$ can be found in Clemens & Mungal (1990), with little changes seen when compared to the $Mc = 0.62$ case.

A final use of the technique is in its application to a possible mixing enhancement. Several studies (e.g. Shau & Dolling, 1989) have attempted to enhance mixing by interaction of a spanwise shock with the two-dimensional mixing layer. While there is a local enhancement, the layer quickly recovers to its slow growth mode. Here we present an alternate technique, the Side Wall Shock Vortex Generator (SWSVG), described in Fig. 11. We have found that placement of a disturbance in the supersonic nozzle, normal to the span as shown, generates an oblique shock wave which upon interacting with the splitter tip generates a streamwise vortex. Figure 12 shows time averaged end views of the flow with (a) no disturbance, (b) one disturbance, and (c) two sidewall disturbances respectively. While the thickness of the layer appears unchanged, the overall mixing volume has increased by about

60%. Clemens & Mungal (1991b) also show that it is possible to change the location of the vortex by movement of the SWSVG within the supersonic nozzle.

3. Conclusions

This work has demonstrated through planar visualizations that low compressibility, high Reynolds number mixing layers continue to show the Brown-Roshko structure seen in incompressible layers. Compressible layers are also seen to be more three-dimensional. These changes are a result of compressibility, and are not a Reynolds number effect.

In addition, it is suggested that shock waves which interact with the splitter plate in a direction normal to the span are better candidates for mixing enhancements than interactions which occur in the spanwise direction.

REFERENCES

CLEMENS, N. T. & MUNGAL, M. G. 1990 Two- and three-dimensional effects in the supersonic mixing layer. *AIAA-90-1978.*

CLEMENS, N. T. & MUNGAL, M. G. 1991a A planar Mie scattering technique for visualizing supersonic mixing flows. To appear, *Expts. Fluids* (1991).

CLEMENS, N. T. & MUNGAL, M. G. 1991b Side-wall shock vortex generator for supersonic mixing enhancement. To appear in *J. Prop. Power* (1991)

PAPAMOSCHOU, D. & ROSHKO, A. 1988 The compressible turbulent shear layer: an experimental study. *J. Fluid Mech.* **197**, 453-477.

SAMIMY, M. & LELE, S. K. 1990 Motion of particles with inertia in a compressible shear layer. Submitted to *Phys. Fluids A*, (1990)

SANDHAM, N. D. & REYNOLDS, W. C. 1989 Growth of oblique waves in the mixing layer at high Mach number. *Turbulent Shear Flows 7,* Stanford University, Paper #9-5.

SHAU, Y. R. & DOLLING, D. S. 1989 Experimental study of spreading rate enhancement of high Mach number turbulent shear layers. *AIAA-89-2458.*

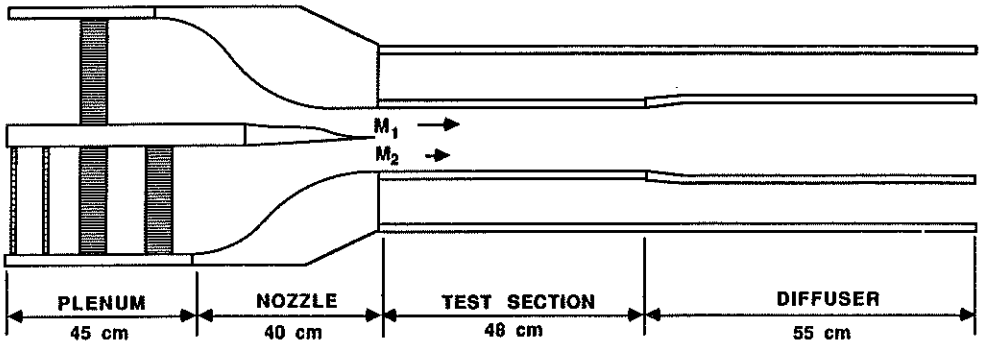

FIGURE 1. Supersonic wind tunnel schematic

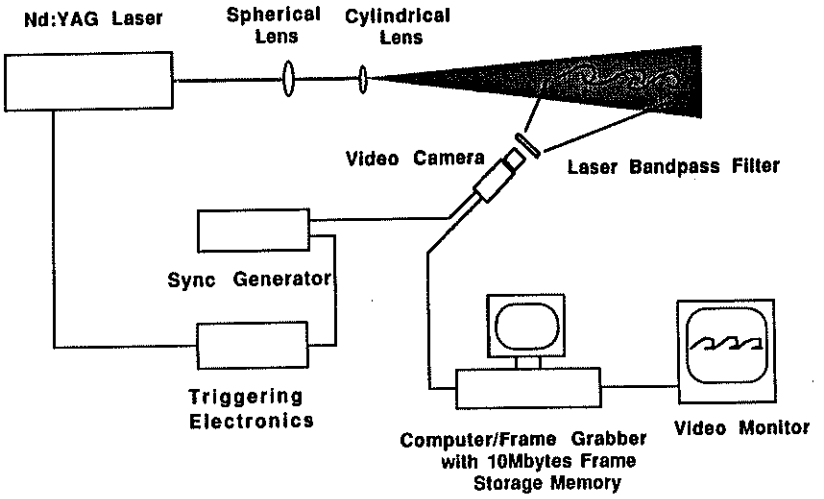

FIGURE 2. Schematic of the imaging setup.

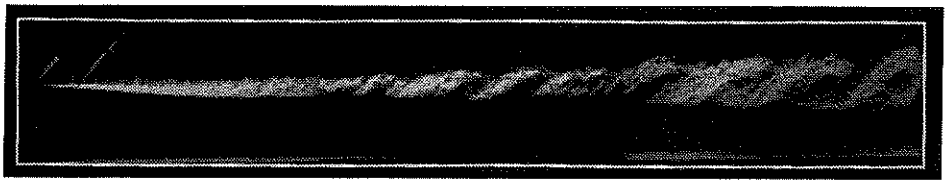

FIGURE 3. Composite schlieren for $Mc = 0.28$, $x = 0 - 45$ cm. Flow is from left to right.

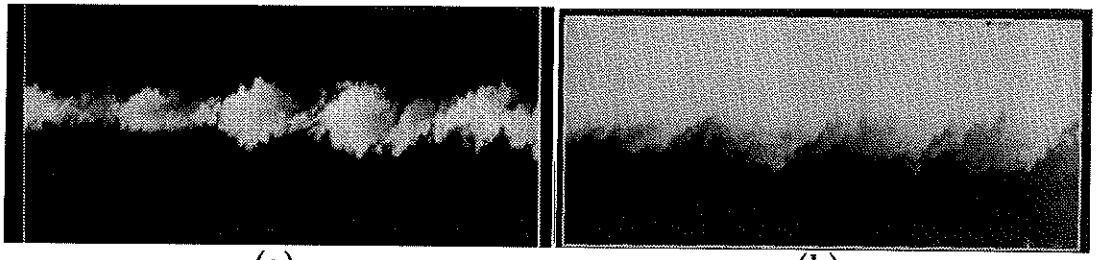

(a) (b)

FIGURE 4. Side view Mie scattering for $Mc = 0.28$, $x = 15 - 28$ cm: (a) product formation method, (b) passive scalar method. Flow is from left to right.

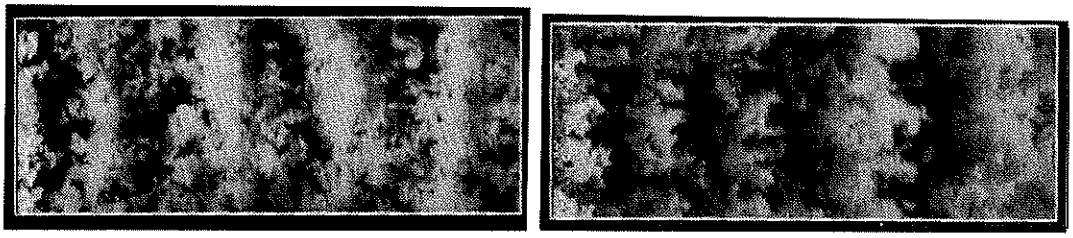

(a) (b)

FIGURE 5. Plan view Mie scattering for $Mc = 0.28$, $x = 15 - 30$ cm: (a) product formation method, (b) passive scalar method. Flow is from left to right.

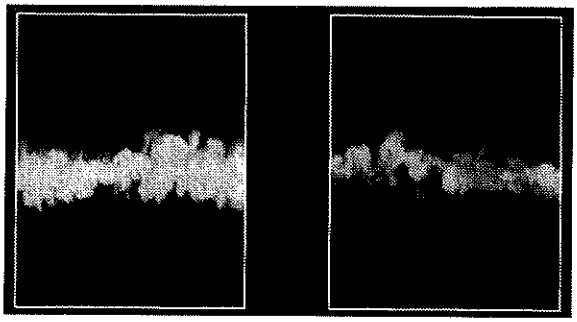

FIGURE 6. Product formation end view Mie scattering images for $Mc = 0.28$, $x = 18$ cm. Image on left shows cut through vortex core, image on right shows cut through braid.

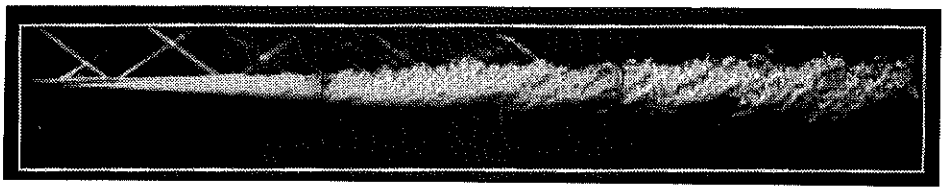

FIGURE 7. Composite schlieren for $Mc = 0.62$, $x = 0 - 45$ cm. Flow is from left to right.

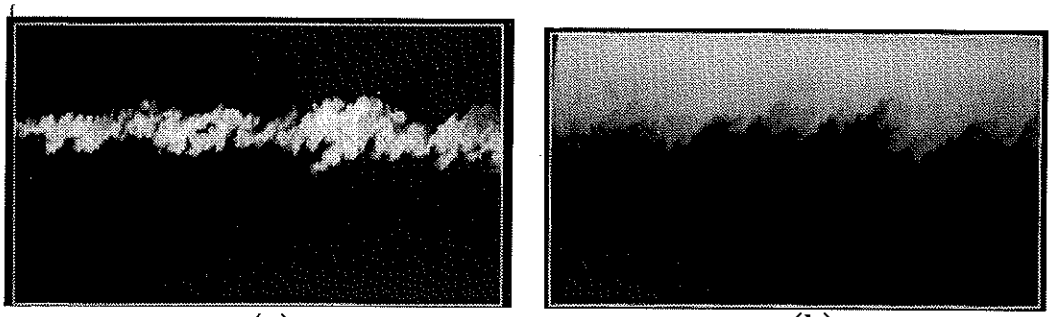

(a) (b)

FIGURE 8. Side view Mie scattering for $Mc = 0.62$, $x = 15 - 28$ cm: (a) product formation method, (b) passive scalar method. Flow is from left to right.

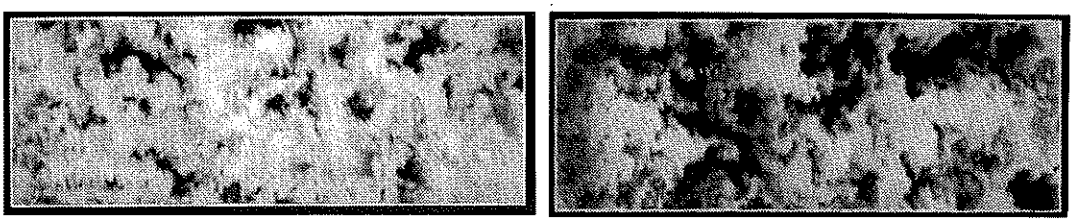

(a) (b)

FIGURE 9. Plan view Mie scattering for $Mc = 0.62$, $x = 15 - 30$ cm: (a) product formation method, (b) passive scalar method. Flow is from left to right.

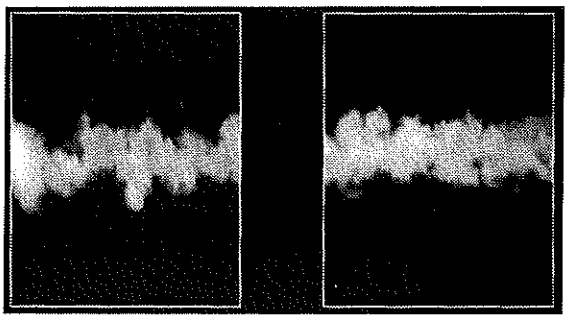

FIGURE 10. Product formation end view Mie scattering images for $Mc = 0.62$, $x = 22$ cm.

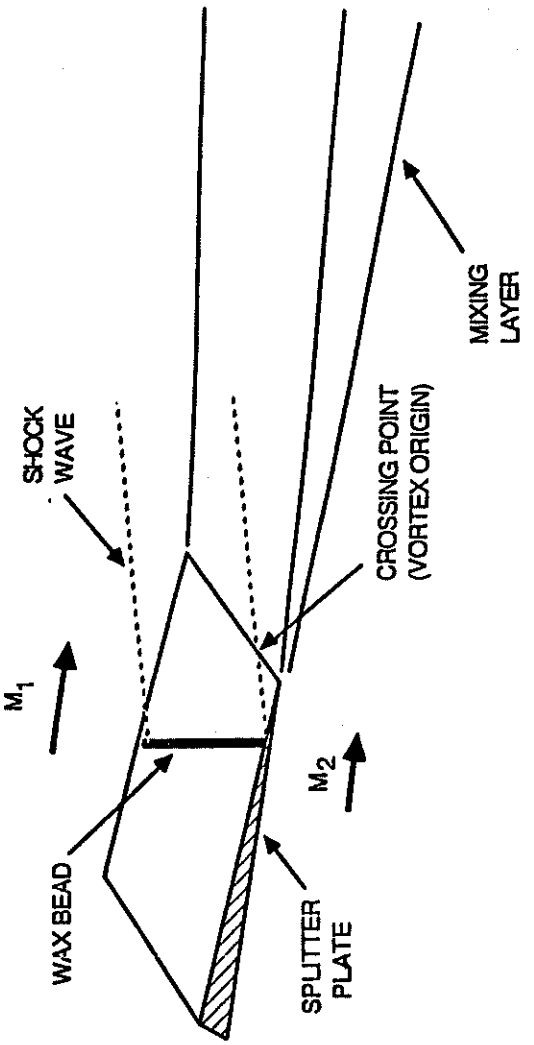

FIGURE 11. Perspective view of the supersonic mixing layer and the SWSVG.

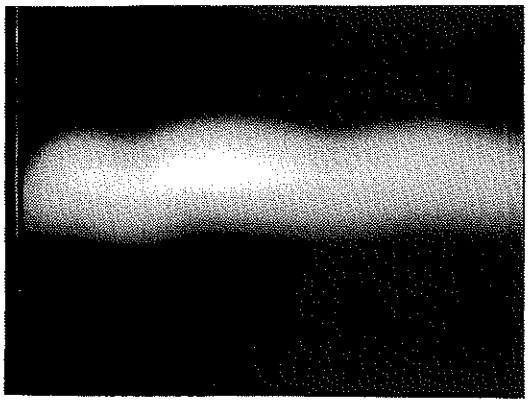

(a)

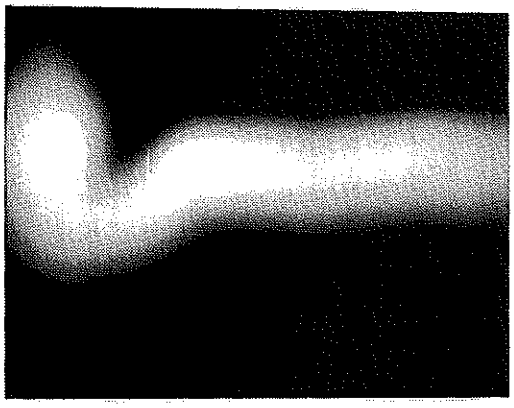

(b)

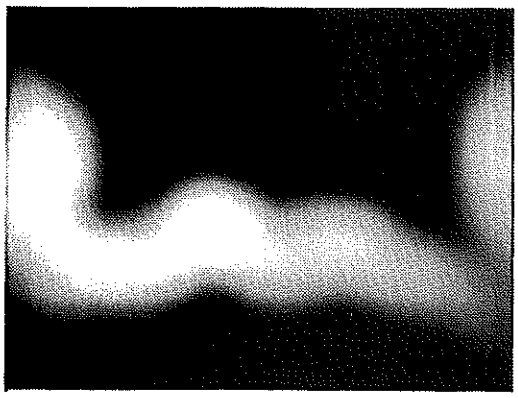

(c)

FIGURE 12. Experimental result: End views of mixed fluid using laser light-sheet visualization for $M_1 = 2$, $M_2 = 0.4$, $M_c = 0.6$. (a) No wax bead. (b) Vortex generator wax bead on left side-wall at the splitter tip produces vortex on the left side. (c) Beads on both sides produce two counterrotating vortices.